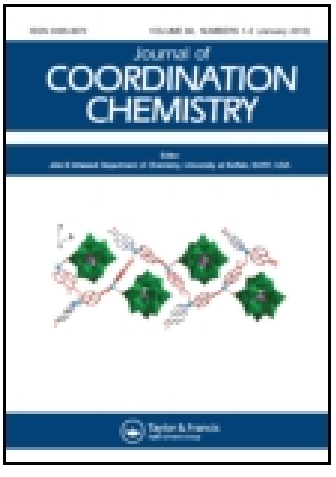

Journal of Coordination Chemistry
Publication details, including instructions for authors and subscription information:
http://www.tandfonline.com/loi/gcoo20

Preparation, surface morphology, and optical properties of indium(III) oxide nanoparticles by thermolysis of indium-poly(vinyl alcohol) coordination polymer

D. Selvakumar[ab], N. Dharmaraj[b], N.S. Kumar[a] & V.C. Padaki[a]

[a] Defence Bioengineering and Electromedical Laboratory, Bangalore, India

[b] Inorganic and Nanomaterials Research Laboratory, Department of Chemistry, Bharathiar University, Coimbatore, India

Accepted author version posted online: 06 Jun 2014.Published online: 03 Jul 2014.

To cite this article: D. Selvakumar, N. Dharmaraj, N.S. Kumar & V.C. Padaki (2014) Preparation, surface morphology, and optical properties of indium(III) oxide nanoparticles by thermolysis of indium-poly(vinyl alcohol) coordination polymer, Journal of Coordination Chemistry, 67:11, 1938-1947, DOI: 10.1080/00958972.2014.932354

To link to this article: http://dx.doi.org/10.1080/00958972.2014.932354

Journal of Coordination Chemistry, 2014
Vol. 67, No. 11, 1938–1947, http://dx.doi.org/10.1080/00958972.2014.932354

Preparation, surface morphology, and optical properties of indium(III) oxide nanoparticles by thermolysis of indium–poly(vinyl alcohol) coordination polymer

D. SELVAKUMAR†‡, N. DHARMARAJ*‡, N.S. KUMAR† and V.C. PADAKI†

†Defence Bioengineering and Electromedical Laboratory, Bangalore, India
‡Inorganic and Nanomaterials Research Laboratory, Department of Chemistry, Bharathiar University, Coimbatore, India

(*Received 25 January 2014; accepted 4 May 2014*)

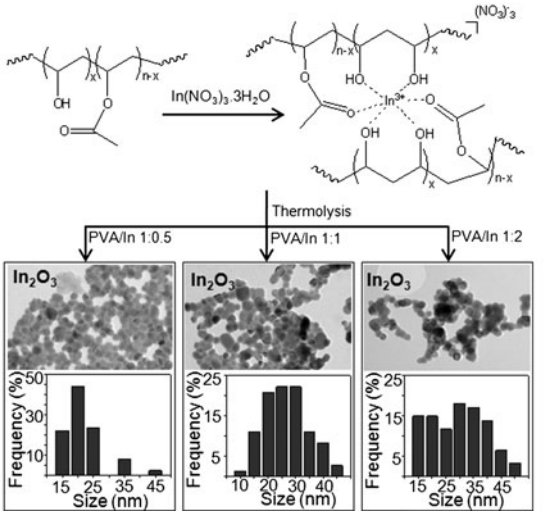

First report on the preparation of well-dispersed, indium(III) oxide (In_2O_3) nanoparticles with 22–35 nm size by polymer thermolysis is presented. Indium–poly(vinyl alcohol) (PVA) coordination polymer films were prepared by 'solution casting technique' from the homogeneous aqueous solution of coordination polymer prepared using PVA and indium(III) nitrate as starting materials; subsequently the films were calcined at 550 °C to yield In_2O_3 nanoparticles. Both indium–PVA coordination polymer that served as the precursor and the titled nanoparticles were characterized by Fourier transform-infrared spectroscopy, photoluminescence (PL), powder X-ray diffraction (XRD), transmission electron microscopy, and thermal analysis. Room temperature PL spectra of the prepared indium oxide nanoparticles showed intense blue emissions around 360, 410 and 430 nm, characteristic of indium oxide nanoparticles due to oxygen vacancies. The lower energy PL emission decreases with an increase of indium(III) content in the precursor. The size of the nanoparticles calculated from line

*Corresponding author. Email: dharmaraj@buc.ac.in

broadening of XRD pattern (cubic; JCPDS: 06-0416) was found to be around 24 nm. The average particle size of the synthesized nanoparticles increased with metal ion content in the precursor coordination polymer.

Keywords: Thermolysis; Indium oxide; Poly(vinyl alcohol); Nanoparticles; Photoluminescence

1. Introduction

Indium(III) oxide (In_2O_3) nanostructures have received attention for their applications in optoelectronic devices, solar cells, liquid crystal displays, biosensors, and gas sensor with high sensitivity to O_3, NO_2, and CO [1–10]. Nanostructured In_2O_3 thin films and powders have been prepared from all three phases (solid phase, liquid phase, and vapor phase) using a wide spectrum of physical and chemical methods [11]. Nanostructured In_2O_3 with interesting morphologies such as nanowire, nanotree, and nanobouquets were prepared by carbon-assisted method involving vapor–liquid–solid mechanism [12]. The size, shape, and dispersion of nanocrystals depend on the method of synthesis. Among solution-based methods such as sol–gel, hydrothermal, co-precipitation, and emulsion routes, sol–gel-mediated synthesis generally yielded highly homogenous nanopowders with good control on the stoichiometric ratio of the final metal oxides [13, 14]. Recently, size-controlled In_2O_3 nanoparticles were prepared by calcinations of In(III) coordination complexes formed using benzenedicarboxylate and benzophenone-4,4-dicarboxylate, respectively [15, 16]. Polyhydroxy alcohol-assisted sol–gel method has been reported for the preparation of polycrystalline $YBa_2Cu_3O_{7-x}$ superconductor nanopowders [17]. In this method, poly(vinyl alcohol) (PVA) chain wraps the metal cations to form sols instead of being dissociated in water and prevents their aggregation, and thus afforded nanomaterials with lower dimensions. Using this strategy, Co_3O_4 nanoparticles with average size of 33 nm were prepared from PVA-coordinated cobalt nitrate through combustion [18]. Polymer-assisted deposition has been demonstrated to produce high quality, simple, as well as complex metal oxide thin films [19–22]. Several metal oxide nanoparticles have been prepared by calcination of electro-spun inorganic–organic composite fibers [23–28]. To the best of our knowledge, no work is reported on the preparation of In_2O_3 nanoparticles using indium-containing coordination polymeric films as a precursor. In this study, we report a convenient method to prepare In_2O_3 nanoparticles by thermolysis of indium–PVA coordination polymer films. The advantages of the present method are: PVA is a good film-forming polymer with multiple –OH groups available for coordination with a range of metal ions to form homogeneous precursor solution; films of coordination polymers are obtained by simple solution casting technique from the homogeneous reaction mixture of polymer-coordinated metal ion solution; the size and dispersity of the final oxide can be varied by adjusting the concentration of reactants. Detailed discussion on the nature of thermal decomposition of the different polymeric precursors (PVA/In) and influence of polymer to metal ion ratio on the formation of In_2O_3 are provided.

2. Experimental

2.1. *Materials and synthesis*

PVA (M_w ~1,25,000, degree of hydrolysis: 98 M%, SD Fine, India) and indium nitrate (Alfa Acer, 99.99%) were used without purification. Transparent polymer films of

PVA-coordinated indium(III) nitrate were prepared using solution casting technique. An aqueous solution of PVA (10% w/w) was prepared by dissolving PVA in water at 80 °C under continuous stirring for 30 min. To a given amount of PVA solution, appropriate quantity of aqueous indium nitrate solution was added and stirred for 5 min using a homogenizer (Miccra D-9, Germany) at 20,000 rpm. During this process, the multiple hydroxyl groups of PVA complexed with indium(III) ions and afforded homogeneous distribution, which in turn prevents precipitation of indium ion from solution [29]. In a previous report, higher concentration of metal ion in the polymer solution resulted in the precipitation of the metal ion without coordination by the polymer completely [17]. The resulting transparent solution was poured into a Petri-plate and dried at 35 °C for 48 h followed by drying in a vacuum oven at 80 °C for 5 h, during which the films turned yellow due to the presence of nitrate. The thickness of the final films was about 200 μm. The as-prepared films were transparent indicating homogeneous complexation of indium ion coordinated by hydroxyl groups of PVA and were calcined in a muffle furnace up to 550 °C for 2 h with a heating rate of 2.5 °C min^{-1} under air to get yellow In_2O_3 nanopowders. The PVA/In coordination polymers prepared with a ratio (wt/wt) of 1 : 0.5, 1 : 1, and 1 : 2 were referred as PVA/In 0.5, PVA/In 1.0 and PVA/In 2.0, respectively, and the corresponding samples of In_2O_3 nanoparticles obtained from the calcination of coordination polymer films were abbreviated as In_2O_3-A, In_2O_3-B, and In_2O_3-C.

2.2. *Characterization methods*

Thermal decomposition behavior of precursor films was studied by thermogravimetry (TGA) using universal V2.5H TA instruments under flow of air (50 mL min^{-1}) at a heating rate of 10 °C min^{-1}. The polymer precursor films were characterized by Fourier transform-Infrared (FT-IR) instrument (Bruker Tensor 27 with ATR accessory) and the obtained spectra were collected and were analyzed using OPUS software. FT-IR spectra of the nanoparticles were obtained as KBr pellets from 4000 to 400 cm^{-1} using a Perkin-Elmer FT-IR 1000 spectrophotometer. Powder X-ray diffraction (XRD) patterns of the samples were recorded using Panalytical X-ray diffractometer (Cu-Kα radiation, $\lambda = 1.54$ Å) employing a scan rate of 0.02° s^{-1} in 2θ range from 10° to 70° and the crystallite size was estimated by the line broadening method. SEM images of the samples were recorded on a JEOL JSM-6490L scanning electron microscope. Transmission electron microscopy (TEM) images were taken using a JEOL JEN 2010 operated at 200 kV accelerating voltage using a copper grid dipped in ethanol-containing dispersed nanoparticles. UV–visible absorption spectra of the samples dispersed in ethanol were recorded with a JASCO-UV–VIS spectrophotometer applying quartz cell of optical length 1 cm at room temperature. The photoluminescence (PL) spectra of the samples were recorded on a JASCO spectrofluorometer with 325 nm excitation line (λ_{ex}: 325 nm) using a 450 W Xenon lamp as the excitation source.

3. Results and discussion

3.1. *Structure and thermolysis of coordination polymers*

Figure 1 shows the FT-IR spectra of pristine PVA and the polymeric precursors with varied concentrations of trivalent indium ion. Generally, PVA contains a trace of polyvinyl acetate

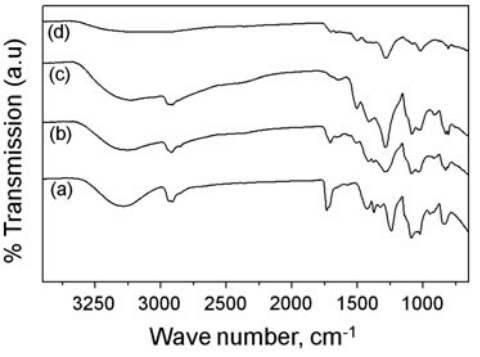

Figure 1. FT-IR spectra of (a) PVA, (b) PVA/In 0.5, (c) PVA/In 1.0 and (d) PVA/In 2.0, respectively.

(PVAc) due to incomplete hydrolysis during its production from PVAc and hence, absorption bands due to acetate were found in addition to alcohol groups. FT-IR spectrum of pristine PVA showed a broad and intense band due to O–H group at 3275 cm^{-1}, which underwent a gradual decrease in its intensity with increasing concentration of indium nitrate, confirming the coordination of alcohol group of PVA with indium. The absorption bands at 2913 and 2851 cm^{-1} are assigned to the asymmetric and symmetric stretches of methylene group of PVA and another band at 1437 cm^{-1} is due to the bending mode of O–H bond [30]. The deformation vibration of alcohol group of PVA at 1239 cm^{-1} nearly disappeared due to the coordination reaction. A band at 1085 cm^{-1} due to C–O was shifted to 1075 cm^{-1}, indicating the coordination of –O–H groups of PVA to indium. The intensity of carbonyl stretching vibration corresponding to the acetate group of PVAc at 1729 cm^{-1} showed a progressive weakening with increasing concentration of indium, confirming the involvement of carbonyl moiety of acetyl in coordination. In addition, bands due to asymmetric and symmetric stretching vibrations of $–NO_2$ groups were present at 1510 and 1290 cm^{-1} of the coordination films [31]. A representative equation to show the complex formed by the coordination of PVA with indium(III) is given in figure 2.

Thermal degradation pattern of the PVA/In performed in air is shown in Supplemental material (figure S1 see online at http://dx.doi.org/10.1080/00958972.2014.932354). A continuous weight loss up to 540 °C was found in the TGA graph of pristine PVA due to the total decomposition of organic moieties in it, whereas the final decomposition temperature of coordination polymers decreased with increasing indium nitrate content. The TGA graphs corresponding to three different precursors viz., PVA/In 0.5, PVA/In 1.0, and PVA/In 2.0 registered three regions of weight loss at 40–150, 150–380, and 380–540 °C. The first and second stages were due to the removal of adsorbed water molecules and degradation of side chains of PVA/PVAc, respectively. The second weight loss is rapid for PVA/In when compared to pristine PVA, attributed to oxidative decomposition of side chains of PVA/PVAc along with the removal of NO_2 and CO_2. The third weight loss is correlated to decomposition of the main chain of PVA [32]. The final decomposition temperature and residues (in wt%) of PVA/In when compared to pristine PVA are shown in Supplemental material (table S1). The decrease in final decomposition temperature with increase of nitrate content confirmed accelerated decomposition of PVA by nitrate. From the decomposition temperature identified from TGA analysis, we have chosen 550 °C as the temperature for calcinations of indium–PVA coordination polymers to yield In_2O_3 nanoparticles.

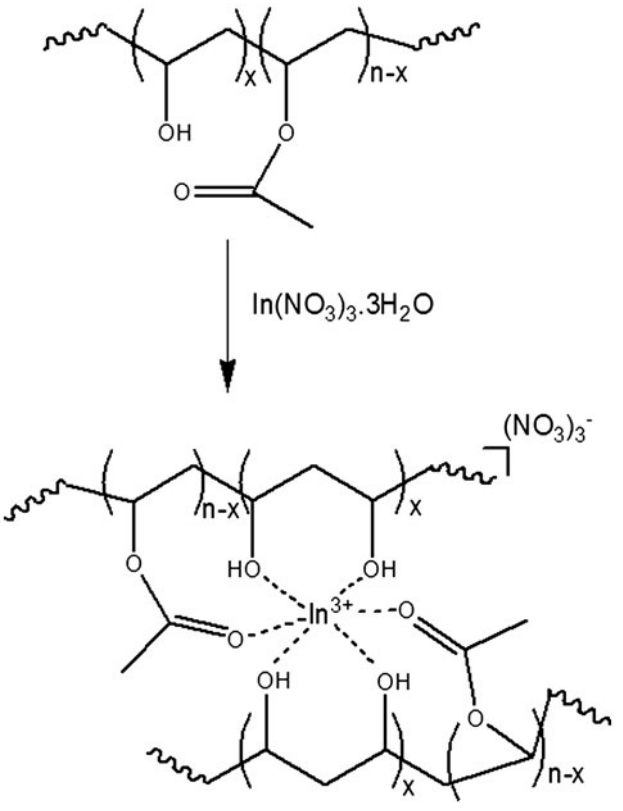

Figure 2. Reaction scheme for the preparation of PVA coordinated indium(III) nitrate.

3.2. *Structural and optical properties of nanoparticles*

The FT-IR spectra of In_2O_3-B calcined at 550 °C and its respective precursor, PVA/In 1.0, are compared in figure 3. After thermolysis, the spectrum did not show any absorptions due to PVA and/or nitrate, indicating their complete removal. However, new absorption bands for In–O bonds appeared at 416 and 561 cm^{-1} [33], supporting the complete removal of organic and/or nitrate during the decomposition process and the formation of pure In_2O_3 nanoparticles. These observations are similar to the preparation on CuO and ZnO nanoparticles by direct calcinations of the respective coordination polymers of Cu(II) and Zn(II), as reported in the literature [34–36].

The UV–visible absorption spectra of In_2O_3 nanoparticles prepared from PVA/In 0.5, PVA/In 1.0 and PVA/In 2.0, respectively, are given in Supplemental material (figure S2). The respective nanoparticles In_2O_3-A, In_2O_3-B, and In_2O_3-C exhibited absorption edge values at 323 nm (4.39 eV), 328 nm (4.32 eV), and 337 nm (4.21 eV). These absorption edges in all the cases were blue shifted when compared to that of bulk In_2O_3 (3.6 eV) as a result of quantum confinement effect [37]. The shift in absorption edges towards lower wavelength suggested that the sizes of the nanoparticles in increasing order are In_2O_3-A, In_2O_3-B, and In_2O_3-C. These absorption edge values are higher than that of In_2O_3 nanoparticles or thin films prepared by solution [38] and vapor deposition route [39], indicating the

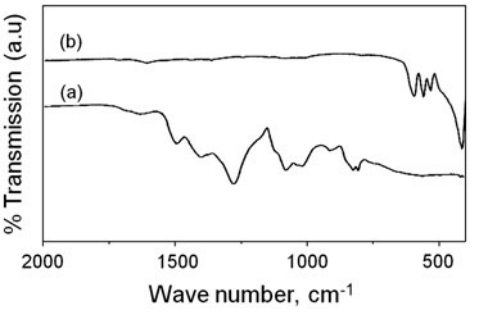

Figure 3. FT-IR spectra of (a) PVA/In 1.0 and (b) In_2O_3-B.

formation of indium(III) oxide nanoparticles with lesser size in our experiment. It can be seen that the absorption edge became broader with increasing the indium content in the coordination polymer. The broadening of absorption edge is associated with increase in size of the nanoparticles as reported earlier [40].

The room temperature PL spectra of the as-prepared In_2O_3 nanoparticles dispersed in ethanol are presented in Supplemental material (figure S3). Bulk In_2O_3 cannot emit light at room temperature [41]. However, nanocrystalline In_2O_3 samples display PL emissions due to oxygen vacancies [42]. All three samples showed emission at 363 nm due to near band emission (NBE) and strong emission near 410, 430 with weak emission around 470 nm from deep level emission (DLE), respectively. The DLE is due to the formation of intraband energy levels as a result of oxygen vacancies. These values are comparable to the already reported values for In_2O_3 nanocrystals [43]. Presence of lower energy absorptions are attributed to impurities and structural defects arising from oxygen vacancies [44, 45]. In our studies, intensities of DLE were higher than NBE owing to higher defect-related emission. The intensity of DLE at 470 nm has appreciably reduced as the concentration of indium ion increases in the polymeric precursor, suggesting decreased oxygen vacancies and structural defects. As was found from thermal studies, the thermal decomposition of PVA was accelerated by nitrate ion present in the polymeric precursor. It is expected that the higher concentration of nitrate would provide an enhanced oxidizing atmosphere and effectively removed the carbonaceous surrounding formed from thermal decomposition of PVA. This mechanism apparently leads to reduced oxygen deficiency, which reduces the intensity of PL emission peaks appearing at lower energy due to oxygen vacancies with respect to increased indium nitrate content in the polymeric precursors.

The formation of nanocrystalline In_2O_3 from thermolysis of polymeric precursors was confirmed by XRD results shown in figure 4. All detectable peaks can be indexed to the cubic phase of the In_2O_3 nanostructure given in the standard material (JCPDS: 06-0416). Moreover, no other diffraction peaks from the impurities or other phases were detected in the XRD pattern, showing very high purity of the prepared In_2O_3 nanoparticles as reported in the preparation of ZnO nanoparticles by calcination of Zn(II) coordination polymers [36, 46]. The crystallite sizes of the nanoparticles were estimated from X-ray line broadening using Scherrer's equation [47]. The average sizes increased as 24, 25, and 26 nm for the In_2O_3 samples prepared, respectively, from PVA/In 0.5n, PVA/In 1.0, and PVA/In 2.0 coordination polymers.

SEM analysis was performed to investigate the morphologies of In_2O_3 nanoparticles formed from the thermolysis of polymeric precursors. It was recently reported that particle size and morphology of In_2O_3 nanoparticles can be varied by simply adjusting the ratio of

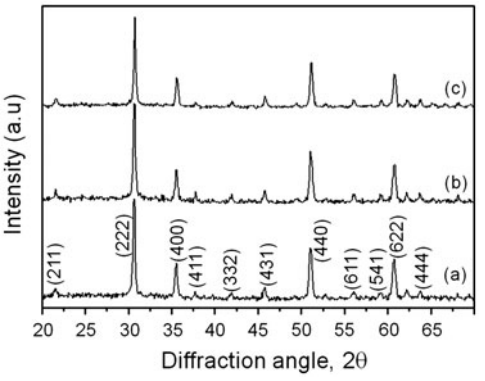

Figure 4. XRD patterns of In_2O_3 prepared using (a) PVA/In 0.5, (b) PVA/In 1.0 and (c) PVA/In 2.0.

reactants in the coordination complexes [14]. Earlier studies showed that the morphology of metal oxide nanoparticles obtained from thermolysis of coordination polymers was greatly influenced by the nature of ligand, geometry of coordination sphere [34, 48], crystal packing of coordination polymers [49], and calcination temperature [50]. The SEM images of the In_2O_3 nanoparticles formed from three PVA/In coordination polymers are given in Supplemental material (figure S4 with respective higher magnifications shown as insets). From the SEM images, the polymeric precursor PVA/In 0.5 yielded In_2O_3 nanoparticles with spherical morphology, whereas, the precursor PVA/In 1.0 afforded agglomerated particles resulting as thin interconnected layers. On the other hand, PVA/In 2.0 polymeric precursor produced thick flake-like materials of indium. It is believed that during the combustion process, evolution of large volume of gasses due to an exothermic reaction between nitrate and the polymer promoted decomposition of over-inflated precursor gel and produced nanoparticles. During the polymer thermolysis, low-density volatile fragments could form small bubbles that grow in size, escape to the surface of the film, and undergo rapid burst to form foam-like structure as reported earlier [51, 52]. With lower concentration of metal ions, the polymer chain completely covers the surface of the nuclei of metal oxide nanocrystals that restricts the contact between the nuclei and thus forms separate particles. With a composition of PVA/In 1.0, presumably, the nuclei of metal oxide nanocrystals aggregate with each other to form a 2-D assembly of particles, leading to an interconnected layer-like structure as identified from SEM images. When the concentration of indium ion is further increased, more In_2O_3 nanocrystals combine with one another and result in a thick flake-like morphology corresponding to the sample obtained by decomposition of PVA/In 2.0 coordination polymer. The SEM studies clearly indicated that the morphology of indium(III) oxide nanoparticles formed was influenced by the ratio between the metal ion and polymer in the coordination polymer precursor.

Further, proof regarding the morphology and particle size of In_2O_3 samples was provided using TEM analysis. The TEM micrographs shown in figure 5 confirmed that the In_2O_3 nanoparticles prepared from all three precursors were spherical. The images are similar to In_2O_3 nanoparticles prepared by thermal decomposition of citrate gel precursor that showed agglomerated nanoparticles of spheroid shape [53]. In the present study, the nanoparticles are progressively agglomerated into branched structures with increasing indium(III) ratio in the precursor polymeric film. Moreover, the particle size distribution obtained from the TEM images also revealed that increasing indium(III) content in the PVA–indium coordination

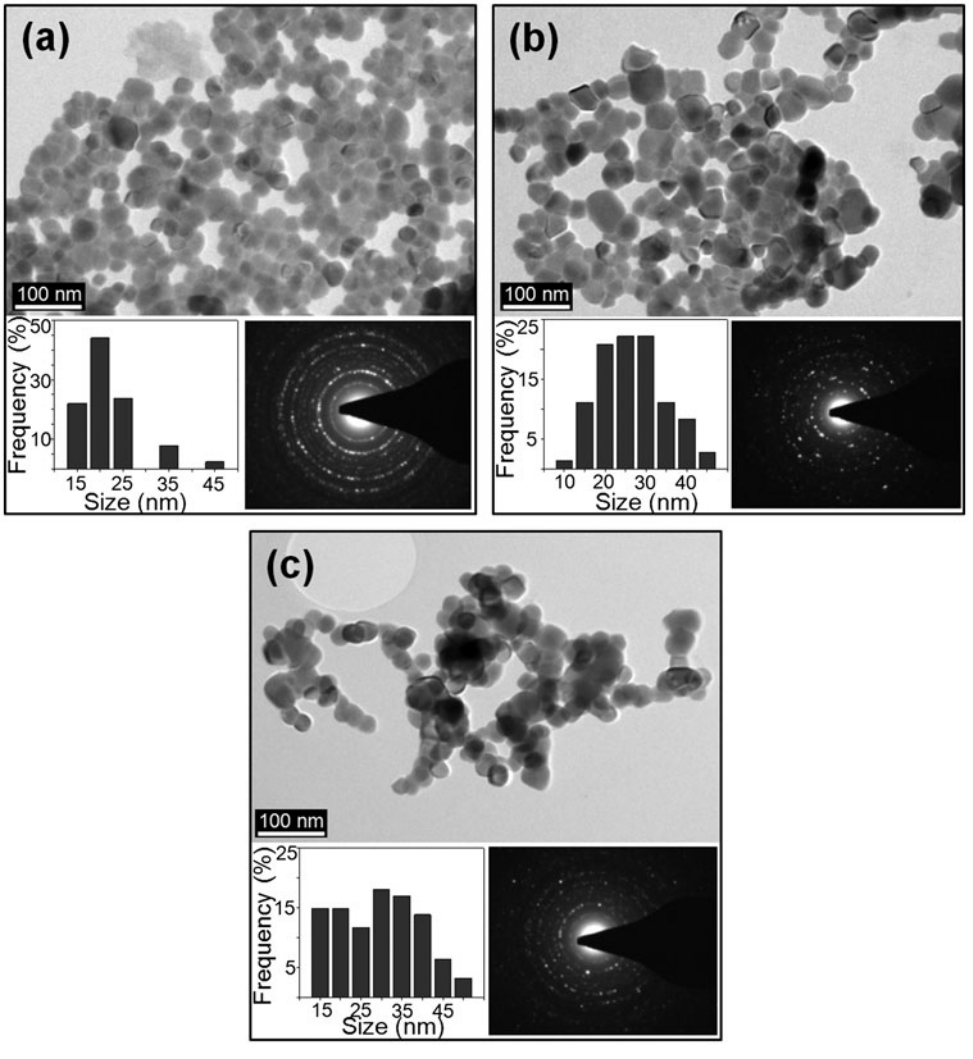

Figure 5. TEM images of In_2O_3 prepared using (a) PVA/In 0.5, (b) PVA/In 1.0 and (c) PVA/In 2.0 with corresponding SAED pattern.

polymer resulted in larger size of nanoparticles. As observed in the SEM images, higher concentration of indium(III) ions leads to enhanced contact between the nanocrystals and hence formed larger particles at the expense of smaller particles similar to the Ostwald ripening process. The corresponding selected area electron diffraction SAED patterns of the three different In_2O_3 samples (In_2O_3-A, In_2O_3-B and In_2O_3-C) showed bright spots revealing their phase pure, cubic crystalline structure.

4. Conclusion

Preparation of phase pure, cubic In_2O_3 nanoparticles by thermolysis of PVA-coordinated indium(III) nitrate polymer is presented. A good comparison between the results of our

work was made with other metal oxide nanoparticles formed by thermal decomposition of suitable coordination precursors in order to strengthen the merit of the research work undertaken herein. Effect of PVA to indium ion ratio on the morphology and size of the as-prepared In_2O_3 nanoparticles were investigated. Powder XRD confirmed the cubic crystalline phase of the In_2O_3 nanoparticles with an average size of 24 nm. Optical and TEM studies revealed that the size of nanoparticles increased with indium(III) content in the coordination polymer. PL studies confirmed that the low-energy emission of oxides gradually disappeared with increasing indium(III) nitrate ratio in the coordination polymer precursors due to an enhanced oxidizing microenvironment during thermolysis.

Acknowledgments

The authors thank Dr K. Kadirvelu, Joint Director Coordinator, DRDO-BU CLS, Bharathiar University, Coimbatore, India, for extending XRD and SEM facilities and Dr D. Bharathimohan, assistant professor in Physics, Pondicherry University, Pondicherry, India, for TEM studies.

References

[1] C.H. Liang, G.W. Meng, Y. Lei, F. Phillipp, L.D. Zhang. *Adv. Mater.*, **13**, 1330 (2001).
[2] X. Lo, M.W. Wanlass, T.A. Gessert, K.A. Emery, T.J. Coutts. *Appl. Phys. Lett.*, **54**, 2674 (1989).
[3] M.J. Zheng, L.D. Zhang, G.H. Li, X.Y. Zhang, X.G. Wang. *Appl. Phys. Lett.*, **79**, 839 (2001).
[4] M. Mazzera, M.Z. Zha, D. Calestani, A. Zappettini, L. Lazzarini, G. Salviati, L. Zanotti. *Nanotechnology*, **18**, 355707 (2007).
[5] C.Q. Wang, D.R. Chen, X.L. Jiao, C.L. Chen. *J. Phys. Chem. C*, **111**, 13398 (2007).
[6] M. Curreli, M. Li, Y.H. Sun, B. Lei, M.A. Gundersen, M.E. Thompson, C.W. Zhou. *J. Am. Chem. Soc.*, **127**, 6922 (2007).
[7] Z.M. Zeng, K. Wang, Z.X. Zhang, J.J. Chen, W.L. Zhou. *Nanotechnology*, **20**, 045503 (2009).
[8] K.I. Choi, H.R. Kim, J.H. Lee. *Sens. Actuators, B*, **138**, 497 (2009).
[9] J.T. McCue, J.Y. Ying. *Chem. Mater.*, **19**, 1009 (2007).
[10] S. Kar, S. Chaudhuri. *Chem. Phys. Lett.*, **422**, 424 (2006).
[11] E.C.C. Souza, J.F.Q. Rey, E.N.S. Muccillo. *Appl. Surf. Sci.*, **255**, 3779 (2009).
[12] K.C. Kam, F.L. Deepak, A.K. Cheetham, C.N.R. Rao. *Chem. Phys. Lett.*, **397**, 329 (2004).
[13] M.M. Bagheri-Mohagheghi, N. Shahtahmasebi, E. Mozafari, M.S. Shokooh-Saremi. *Physica E*, **41**, 1757 (2009).
[14] W.S. Seo, H.H. Jo, K. Lee, J.T. Park. *Adv. Mater.*, **15**, 795 (2003).
[15] L.N. Jin, Q. Liu, W.Y. Sun. *CrystEngComm.*, **15**, 4779 (2013).
[16] L.N. Jin, Q. Liu, W.Y. Sun. *Mater. Lett.*, **102–103**, 112 (2013).
[17] Y.K. Sun, I.H. Oh. *Ind. Eng. Chem. Res.*, **35**, 4296 (1996).
[18] J. Jiu, Y. Ge, X. Li, L. Nie. *Mater. Lett.*, **54**, 260 (2002).
[19] Y. Hao, J. Quanxi, W. Haiyan. *Integr. Ferroelectr.*, **100**, 132 (2008).
[20] Q.X. Jia, T.M. McCleskey, A.K. Burrell, Y. Lin, G.E. Collis, H. Wang, A.D.Q. Li, S.R. Foltyn. *Nat. Mater.*, **3**, 529 (2004).
[21] D. Li, Q.X. Jia. Polymer-assisted aqueous deposition of metal oxide films, US Patent No. 6589457 (2003).
[22] M.A. Garcia, M.N. Ali, T. Parsons-Moss, P.D. Ashby, H. Nitsche. *Thin Solid Films*, **516**, 6261 (2008).
[23] D. Lin, H. Wu, R. Zhang, W. Pan. *Nanotechnology*, **18**, 465301 (2007).
[24] S.K. Lim, S.H. Hwang, D. Chang, S. Kim. *Sens. Actuators, B*, **149**, 28 (2010).
[25] N. Dharmaraj, H.C. Park, C.K. Kim, H.Y. Kim, D.R. Lee. *Mater. Chem. Phys.*, **87**, 5 (2004).
[26] N. Dharmaraj, C.H. Kim, K.W. Kim, H.Y. Kim, E.K. Suh. *Spectrochim. Acta, Part A*, **64**, 136 (2005).
[27] S. Shukla, E. Brinley, H.J. Cho, S. Seal. *Polymer*, **46**, 12130 (2005).
[28] K. Methira, S. Pitt, W. Sujitra. *Mater. Chem. Phys.*, **119**, 175 (2010).
[29] S.K. Saha, A. Pathak, P. Pramanik. *J. Mater. Sci. Lett.*, **14**, 35 (1995).
[30] K. Nakamoto. *Infrared and Raman Spectra of Inorganic and Coordination Compounds*, 4th Edn, p. 24, Wiley Interscience, New York (1986).

[31] N.B. Colthup, L.H. Daly. *Introduction to Infrared and Raman Spectroscopy*, 3rd Edn, Academic Press, New York (1990).
[32] G.M. Kim, A.S. Asran, G.H. Michler, P. Simon, J.S. Kim. *Bioinspir. Biomim.*, **3**, 046003 (2008).
[33] C. Chen, D. Chen, X. Jiao, C. Wang. *Chem. Commun.*, **44**, 4632 (2006).
[34] A. Mehrani, A. Morsali, P. Ebrahimpour. *J. Coord. Chem.*, **66**, 856 (2013).
[35] R. Gupta, S. Sanotra, H.N. Sheikh, B.L. Kalsotra, V.K. Gupta, V. Rajnikant. *J. Coord. Chem.*, **65**, 3917 (2012).
[36] A. Hosseinian, S. Jabbari, A.R. Mahjoub, M. Movahedi. *J. Coord. Chem.*, **65**, 2623 (2012).
[37] C. Lee, M. Kim, T. Kim, A. Kim, J. Paek, J. Lee, S. Choi, K. Kim, J. Park, K. Lee. *J. Am. Chem. Soc.*, **128**, 9326 (2006).
[38] S. Maensiri, P. Laokul, J. Klinkaewnarong, S. Phokha, V. Promarak, S. Seraphin. *J. Optoelectron. Adv. Mater.*, **10**, 161 (2008).
[39] S.K. Chong, S.N.A. Azizan, K.W. Chan, H.Q. Nguyen, W.S. Chiu, Z. Aspanut, C.F. Dee, S.A. Rahman. *Nanoscale Res. Lett.*, **8**, 428 (2013).
[40] L. Wang, X.T. Tao, J.X. Yang, Y. Ren, Z. Liu, M.H. Jiang. *Opt. Mater.*, **28**, 1080 (2006).
[41] Y. Ohhata, F. Shinoki, S. Yoshida. *Thin Solid Films*, **59**, 255 (1979).
[42] H. Cao, X. Qiu, Y. Liang, Q. Zhu. *Appl. Phys. Lett.*, **83**, 761 (2003).
[43] P.G. Pani, G. Aharon. *Eur. J. Inorg. Chem.*, **6**, 919 (2008).
[44] Y.C. Kong, D.P. Yu, B. Zhang, W. Fang, S.Q. Feng. *Appl. Phys. Lett.*, **78**, 407 (2001).
[45] D.M. Bagnall, Y.F. Chen, Z. Zhu, T. Yao, M.Y. Shen, T. Goto, T. Goto. *Appl. Phys. Lett.*, **73**, 1038 (1998).
[46] K.A. Siddiqui, G.K. Mehrotra. *J. Coord. Chem.*, **66**, 1746 (2013).
[47] B.D. Cullity, S.R. Stock. *Elements of X-ray Diffraction*, 3rd Edn, Prentice Hall, Upper Saddle River, NJ (2001).
[48] S. Khanjani, N. Soltanzadeh, R. Sabahi, A. Morsali, S.W. Joo. *J. Coord. Chem.*, **66**, 3391 (2013).
[49] F. Bigdeli, A. Morsali, P. Retailleau. *Polyhedron*, **29**, 801 (2010).
[50] M. Thirumavalavan, K.L. Huang, J.F. Lee. *Materials*, **6**, 4198 (2013).
[51] I.S. Wichman. *Combust. Flame*, **63**, 217 (1986).
[52] J.E.J. Staggs. *Fire Saf. J.*, **34**, 69 (2000).
[53] J.F.Q. Rey, T.S. Plivelic, R.A. Rocha, S.K. Tadokoro, I. Torriani, E.N.S. Muccillo. *J. Nanopart. Res.*, **7**, 203 (2005).